NANO: Brief Reports and Reviews
Vol. 10, No. 8 (2015) 1550117 (9 pages)

DOI: 10.1142/S1793292015501179

World Scientific
www.worldscientific.com

Analysis of Localized Surface Plasmon Resonance in Ag/ITO/CdS/SiO_2 Multilayered Nanostructured Composite

Chao Liu, Jingwei Lv, Famei Wang, Qiang Liu and Haiwei Mu*
School of Electronics Science, Northeast Petroleum University
Daqing 163318, P. R. China
**mhwmzh@163.com*

Tao Sun†
Institute of Microelectronics, Agency for Science
*Technology and Research (A*STAR), 117685, Singapore*
†*taosun@hotmail.com.hk*

Qiang Liu
School of Science, Harbin Engineering University
Harbin 150001, P. R. China
liuqiang38074517@126.com

Paul K. Chu
Department of Physics and Materials Science
City University of Hong Kong
Hong Kong 999077, P. R. China
ljw_0816@163.com

Received 5 May 2015
Accepted 15 July 2015
Published 4 September 2015

Multilayered nanoshells have attracted much attention due to their unique optical, electronic and magnetic properties. In this work, numerical calculation using discrete dipole approximation (DDA) is conducted to investigate the quad-layered metal nanoshell consisting of a particle with a dielectric silica (SiO_2) core, inner cadium sulfide (CdS) shell, middle indium tin oxide (ITO) shell and outer metal silver (Ag) shell. The phenomenon is interpreted by plasmon hybridization theory and the Ag–ITO–CdS–SiO_2 multilayered nanoshells are studied by extinction spectra of localized surface plasmon resonance. The variation in the spectrum peak with nanoparticle thickness and refractive index of the surrounding medium is derived. The electric field enhancement contour around the nanoparticles under illumination is analyzed at the plasmon resonance wavelength. The $|\omega_-^-\rangle$, $|\omega_-^+\rangle$, and $|\omega_+^-\rangle$ modes red-shift with the refractive index of the surrounding medium and increase in the layer thickness causes either blue-shift or red-shift as shown by the extinction spectra. The mechanism of the red-shift or blue-shift is discussed. The $|\omega_-^-\rangle$ mode blue-shifts and furthermore, the $|\omega_+^-\rangle$ and $|\omega_-^+\rangle$ modes of the Ag coated multilayered nanostructure are noticeable by comparing the extinction efficiency spectra of the Au–ITO–CdS–SiO_2 and Ag–ITO–CdS–SiO_2 multilayered nanoshells.

*,†Corresponding authors.

Keywords: Localized surface plasmon resonance; multilayered nanoshells; discrete dipole approximation; plasmon hybridization.

1. Introduction

Noble metal nanostructures have great potential in the areas of nanomedicine, biosensing and food safety due to their localized surface plasmon resonance (LSPR) properties.[1–3] Surface plasmons are collective excitations of the electrons at the interface between a conductor and an insulator and are described by evanescent electromagnetic waves that are not necessarily located at the interface.[4–6] The properties of LSPR depend largely on the shape and size of the nanoparticles as well as the refractive index of the surrounding medium.[7,8] The optical responses associated with LSPR in metallic nanoparticles with different structures have been investigated[9] and it is known that only one plasmonic resonance peak is generated from spherical nanoparticles, while two or more plasmonic resonance peaks can occur in other kinds of nanostructures such as nanodimers, nanorods and core/shell structures.[10–12]

Recent research has focused on multilayered metallic–dielectric nanostructures that exhibit multiple resonance peaks capable of detecting various types of targets on one sample at the same time.[7] The tunable intensity and peak wavelength of LSPR arising from layered metallic–dielectric nanostructures render them versatile by combining with different materials. Su[13] studied the LSPR optical response of Au/SiO_2 mutilayered nanodisks possessing distinct properties by controlling the dielectric layer thickness and Qian[14] investigated the optical properties induced by dual symmetry breaking in the gold–silica–gold multilayered nanoshells. By controlling the two types of symmetry breaking, polarization-dependent multiple plasmon resonance is observed. Therefore, the LSPR properties of Ag-coated multilayered nanoshells with other materials are interesting. Among various types of dielectric materials, SiO_2 is one of the most extensively studied and used due to its unique optical and electrical properties.[15] Indium tin oxide (ITO) has the advantages of near-metallic conductivity,[16] environmental stability,[17] and high transparency in the visible region[18] and cadmium sulfide (CdS) is often utilized in luminescence probes and photosensors.[19] However, the LSPR properties of nanoshells with multilayered structure of these materials are relatively not well known.

In this work, quad-layer metallic nanostructures consisting of metal Ag, ITO, CdS and SiO_2 are proposed and the effects of the layer thickness and the refractive index of the surrounding medium on the LSPR properties of Ag–ITO–CdS–SiO_2 multilayered nanoshells are studied by the discrete dipole approximation (DDA) method. In addition, the electric field enhancement contour around the multilayered nanoshells is analyzed on the basis of the plasmon hybridization theory.[20]

2. Theory

The isolated concentric Ag–ITO–CdS–SiO_2 multilayered nanostructure is modeled as shown in Fig. 1. The core SiO_2 has a radius r_1 and the thicknesses of the inner shell, middle shell, and outer shell are $r_2 - r_1, r_3 - r_2$ and $r_4 - r_3$, respectively. The dielectric constants of the inner dielectric core, inner shell, middle shell and outer silver shell are ε_1, ε_2, ε_3 and ε_4. The surrounding medium has a refractive index of n and DDA is carried out to simulate the LSPR properties of multilayered nanostructures.

The numerical approach of DDA is widely used to calculate the electromagnetic field distribution of arbitrary structure, shape and size. The scattering spectra, absorption spectra and extinction spectra of these nanoparticles can be calculated by DDA as well. In DDA, the target can be measured by a cubic array of N polarizable points.[21,22] Generally, the

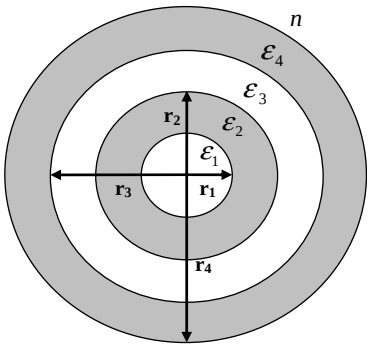

Fig. 1. Schematic representation of the concentric multilayered nanosphere.

continuum target can be substituted by the discrete dipoles as long as the dipole number N is large enough. The polarization vector is generated by the interaction between the arbitrary point dipole and local electric field $\mathbf{E}_{\text{loc}}$ so that

$$\mathbf{P}_i = \alpha_i \cdot \mathbf{E}_{\text{loc}}(\mathbf{r}_i), \tag{1}$$

where α_i is the tensor of polarizability of the point dipole, $\mathbf{r}_i$ is the central position and $\mathbf{E}_{\text{loc}}$ consists of the electric field $\mathbf{E}_{\text{inc},i}$ at position j due to the incident plane wave and electric field stimulated by $(N-1)$ other dipoles as shown in the following:

$$\mathbf{E}_{\text{inc},i} = \mathbf{E}_0 \exp i(\mathbf{k}\cdot\mathbf{r}_i - \omega t) \tag{2}$$

$$\mathbf{E}_{\text{other},i} = -\sum_{j\neq i} \mathbf{A}_{ij}\cdot\mathbf{P}_j, \tag{3}$$

where $\mathbf{E}_0$ and $\mathbf{k}$ represent the amplitude and wave vector of the incident wave, respectively, $|\mathbf{k}| = \omega/c$, and $-\mathbf{A}_{ij}\cdot\mathbf{P}_j$ is the contribution to the electric field at position i due to the dipole at position j as follows:

$$\mathbf{A}_{ij}\cdot\mathbf{P}_j = \frac{\exp(ik\mathbf{r}_{ij})}{\mathbf{r}_{ij}^3} \times \left\{ \begin{array}{l} k^2\mathbf{r}_{ij}\times(\mathbf{r}_{ij}\times\mathbf{P}_j) + \dfrac{(1-ik\mathbf{r}_{ij})}{\mathbf{r}_{ij}^2} \\ \times[\mathbf{r}_{ij}^2\mathbf{P}_j - 3\mathbf{r}_{ij}(\mathbf{r}_{ij}\cdot\mathbf{P}_j)] \end{array} \right\}, \quad (i\neq j) \tag{4}$$

where $\mathbf{r}_{ij} = |\mathbf{r}_i - \mathbf{r}_j|$. Equation (4) serves to define the matrices $\mathbf{A}_{ij}$ for $i \neq j$. It can be defined as

$$\mathbf{A}_{ij} = \boldsymbol{\alpha}_i^{-1}, \tag{5}$$

so that the scattering problem can be briefly described as a set of N inhomogeneous linear complex vector equations as follows:

$$\sum_{j=1}^{N} \mathbf{A}_{ij}\cdot\mathbf{P}_j = \mathbf{E}_{\text{inc},i}(i = 1, 2, \ldots, N). \tag{6}$$

If the polarization $\mathbf{P}_j$ is known, the absorption cross section for the entire grain is

$$C_{\text{abs}} = \frac{4\pi k}{|\mathbf{E}_{\text{inc}}|^2}\sum_{i=1}^{N}\left\{\text{Im}[\mathbf{P}_i\cdot(\boldsymbol{\alpha}_i^{-1})^*\mathbf{P}_i^*] - \frac{2}{3}k^3\mathbf{P}_i\cdot\mathbf{P}_i^*\right\}, \tag{7}$$

The extinction cross section is obtained by the optical theorem[23]

$$C_{\text{ext}} = \frac{4\pi k}{|\mathbf{E}_0|^2}\sum_{j=1}^{N}\text{Im}(\mathbf{E}_{\text{inc},j}^*\cdot\mathbf{P}_j). \tag{8}$$

The extinction efficiency can be expressed as

$$Q_{\text{ext}} = C_{\text{ext}}/\pi\alpha_{\text{eff}}^2, \tag{9}$$

where α_{eff} is the effective radius.

The number of polarizable points should be large enough to minimize the calculation error. In this study, the multilayered nanoshells consisting of Ag, ITO, CdS and SiO_2 are represented by a finite array of polarizable points with the corresponding dielectric constants obtained from Ref. 24.

3. Results and Discussion

3.1. *Effects of refractive index of surrounding medium on extinction spectra*

The extinction spectra of LSPR are influenced by the refractive index of the surrounding medium. A detailed analysis is carried out to obtain the relationship between the extinction spectra and refractive index. Figure 2 shows the extinction spectra of the Ag–ITO–CdS–SiO_2 multilayered nanostructure. Specifically, the parameters $[r_1, r_2 - r_1, r_3 - r_2, r_4 - r_3] = [25, 5, 10, 10]$ nm and $[n_1, n_2, n_3, n_4, n_5, n_6] = [1.0, 1.16, 1.33, 1.41, 1.52, 1.67]$ of the Ag-coated ITO–CdS–SiO_2 multilayered nanoshells are used in the calculation. The dipole resonance wavelength red-shifts from 595 nm to 790 nm when the refractive index varies from 1.0 to 1.67. Similarly, the quadrupole and octupole resonance wavelengths red-shift as the refractive index increases. However, the peak at 260 nm blue-shifts slightly due to the electronic transition of the Ag^+ ions thus producing absorption bands at 200 nm and 230 nm, whereas the electronic transition of metallic Ag^0 appears in the spectral range between 250 nm and 330 nm.[25–27]

Figure 2 shows that there are three plasmonic resonance peaks in the extinction spectrum for a surrounding medium with a refractive index of 1.52, dipole resonance of 740 nm, quadrupole resonance of 570 nm and octupole resonance of 340 nm. Similar results have been obtained from a tunable plasmonic nanoparticle consisting of a metallic silver

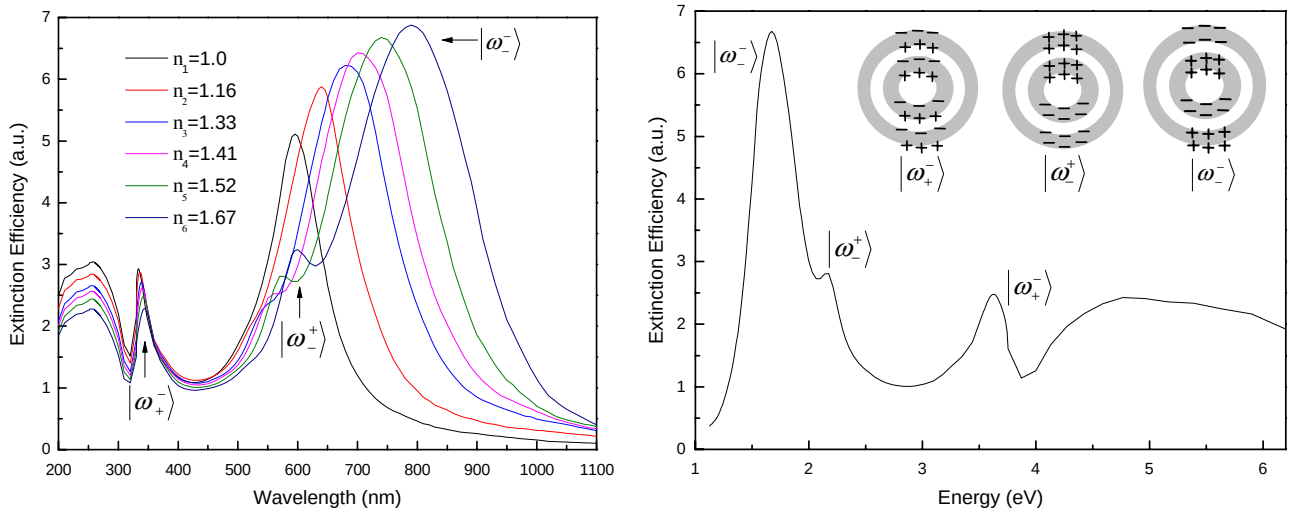

(a) (b)

Fig. 2. (a) Extinction spectra of the Ag–ITO–CdS–SiO_2 multilayered nanostructure as a function of refractive index of the surrounding medium; (b) Extinction spectra of the three types of plasmonic coupling modes based on the LSPR of the Ag–ITO–CdS–SiO_2 multilayered nanostructure.

shell and dielectric SiO_2 core.[28–30] The plasmon resonance of the Ag–ITO–CdS–SiO_2 multilayered structure can be visualized as hybridization between the outer Ag shell plasmon resonance and inner compound shell plasmon mode. The interaction between the inner and outer shells gives rise to two new plasmon resonances: a lower-energy mode ω_- and a higher-energy mode ω_+, corresponding to the symmetric coupling mode and anti-symmetric coupling mode. Theoretically, four plasmon oscillation modes exist as the energy increases: a symmetric bonding mode ω_-^+, an anti-symmetric bonding mode ω_-^-, a symmetric anti-bonding mode ω_+^- and an anti-symmetric anti-bonding mode ω_+^+.

The total extinction spectrum including three types of plasmonic coupling modes with a surrounding medium refractive index of 1.52 is shown in Fig. 2(b). The differences in the dipole moments of the various plasmon modes influence the plasmon couples in the optical field, which is reflected by the magnitude of the extinction resonance for the various modes.[28] The resonance peaks attributed to the three plasmon modes (ω_+^-, ω_-^+, ω_-^-) that are visible at approximately 3.62 eV, 2.17 eV and 1.67 eV or at a wavelength of 340 nm, 570 nm and 740 nm, respectively. However, it should be emphasized that the extinction peak corresponding to the ω_+^+ mode is too weak to observe.

Figure 3(a) depicts the energy level diagram of the plasmon mode of the Ag–ITO–CdS–SiO_2 multilayered nanostructure further showing the interaction between the inner and outer nanoshell plasmons. The anti-symmetric plasmon mode ω_-^- has a lower energy and a smaller dipole moment than the symmetrically polarized hybrid plasmon ω_+^-. The induced polarization of the concentric nanoshell modes is shown in Fig. 3(b). The ω_+^+ mode has the highest energy due to the increased electrostatic repulsion at its internal adjacent interfaces for the plasmon excitation. Furthermore, for the ω_+^+ mode, the sphere plasmon of the inserted sphere oppositely aligns the cavity plasmon with the sphere plasmon to further weaken the dipole moment in the ω_+^+ mode.[31]

3.2. *Distribution of electric field*

Figure 4 presents the contours of the electric field enhancement of the Ag–ITO–CdS–SiO_2 multilayered nanostructure at different resonance wavelengths for a surrounding medium with the refractive index of 1.52. At 260 nm, the electric field is concentrated in the region outside the multilayered nanostructure and CdS inner shell, whereas the electric fields in the SiO_2 core shell, ITO middle shell and Ag outer shell are low, as shown in Fig. 4(a). At 340 nm, the intensity of electric field is mainly distributed in the Ag outer shell, whereas the electric fields in the SiO_2 core–shell and ITO middle shell are weak as shown in Fig. 4(b). Owing to negative and

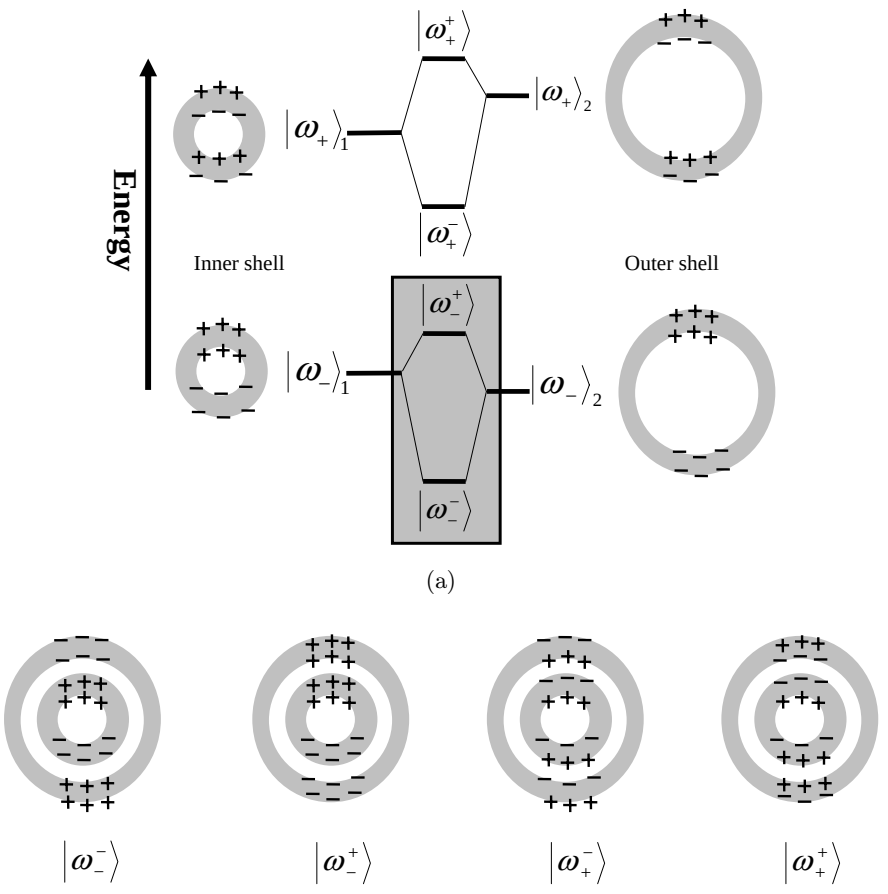

Fig. 3. (a) Energy level diagram of the plasmon modes of multilayered nanoshell; (b) Induced polarizations of the concentric nanoshell modes.

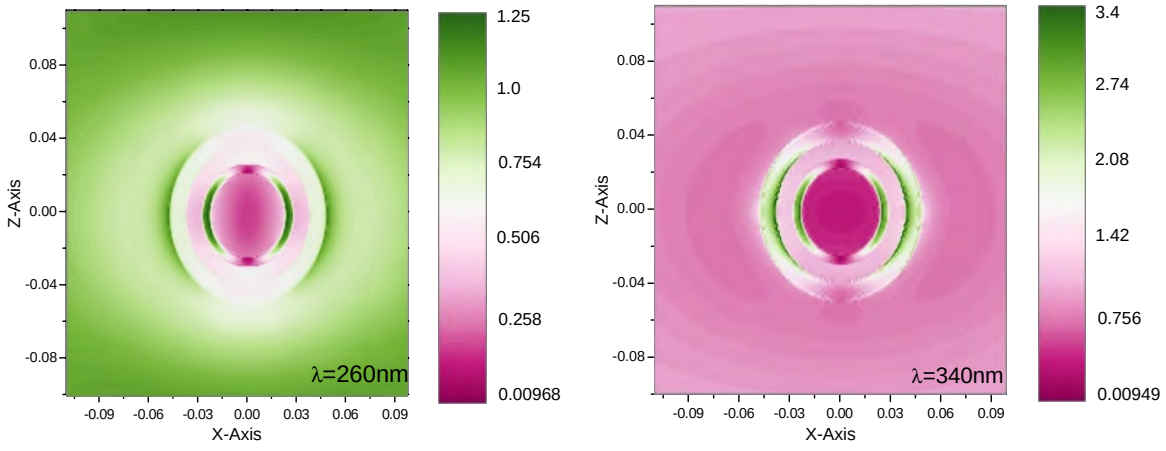

Fig. 4. Electric field enhancement contour around Ag–ITO–CdS–SiO_2 multilayered nanostructure under illumination at plasmon resonance wavelength.

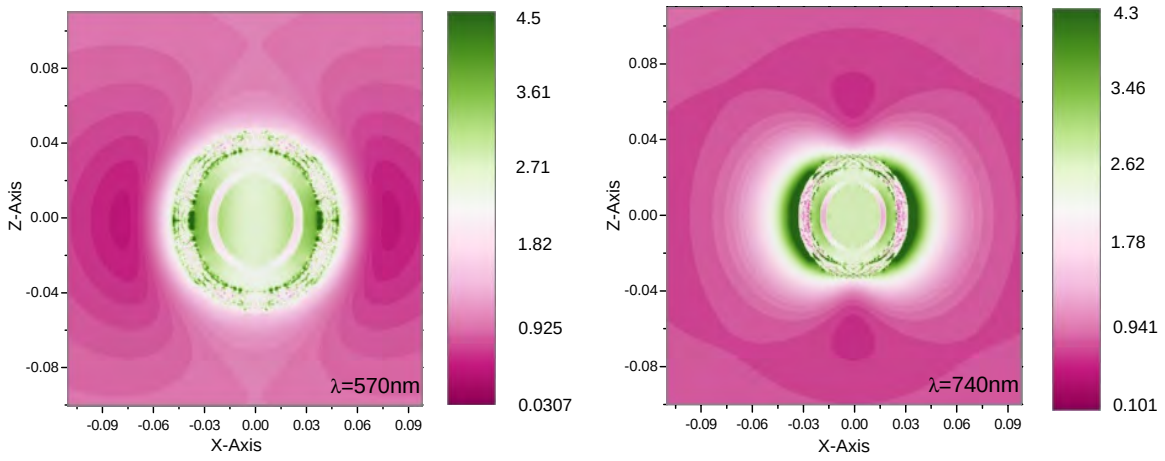

(c) (d)

Fig. 4. (*Continued*)

positive surface charges on the two interfaces of the outer silver shell, intense electric field enhancement occurs on both sides.[32] Accordingly, the extinction peak at 340 nm corresponds to the $|\omega_+^-\rangle$ mode derived from the symmetric coupling between the anti-bonding Ag shell plasmon mode and the inner plasmon.

Figure 4(c) describes the electric field enhancement with $\lambda = 570$ nm. The electric field spreads around the SiO_2 core shell and ITO middle shell. In contrast, the fields in the Ag outer shell and CdS inner shell are very weak. The same negative or positive charges are marked on the inner and outer surfaces of the core and middle shell because the electric field enhancement arises from the poles along the y-axis direction.[7] The extinction peak at 570 nm corresponding to the $|\omega_-^+\rangle$ mode originates from symmetric coupling between the bonding Ag shell plasmon mode and inner plasmon. Similarly, as shown in Fig. 4(d), the electric field still spreads around the SiO_2 core–shell and ITO middle shell with $\lambda = 740$ nm and the contours of the electric field enhancement is pronounced outside the multilayered nanostructure. On the contrary, the fields in the Ag outer shell and CdS inner shell are very weak. Different negative or positive charges are assigned to the inner and outer surfaces of the core and middle shell because the electric field enhancement emerges in the poles along the x-axis direction. According to Fig. 4(b), it can be concluded that the extinction peak at 740 nm corresponds to the $|\omega_-^-\rangle$ mode ascribed to anti-symmetric coupling between the bonding Ag shell plasmon mode and inner plasmon.

3.3. *Comparison of various metal-coated nanostructures*

To compare the optical properties of various metal-coated multilayered nanostructures, the extinction spectra of the Au–ITO–CdS–SiO_2 and Ag–ITO–CdS–SiO_2 multilayered nanoshells are investigated as shown in Fig. 5. The parameters of Ag and Au coated ITO–CdS–SiO_2 multilayered nanoshells are: $[r_1, r_2 - r_1, r_3 - r_2, r_4 - r_3] = [25, 5, 10, 10]$ nm and

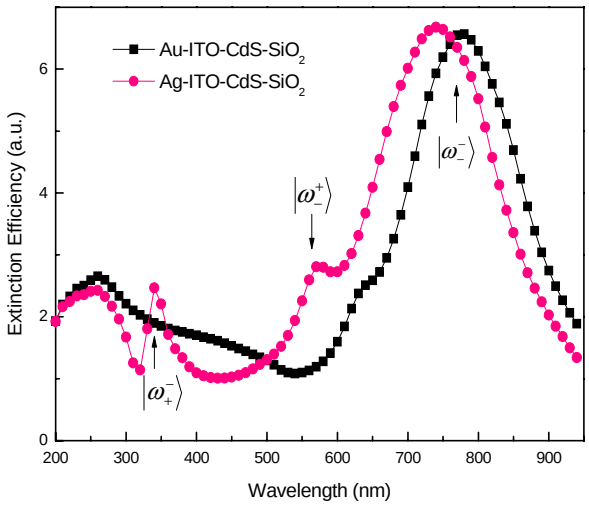

Fig. 5. Comparison of the extinction spectra: Au–ITO–CdS–SiO_2 and Ag–ITO–CdS–SiO_2 multilayered nanoshells as a function of refractive index of the surrounding medium.

$n = 1.52$ in the calculation. The $|\omega_-^-\rangle$ mode of the Ag-coated ITO–CdS–SiO_2 nanoshells blue-shifts compared with Au coated ITO–CdS–SiO_2 nanoshells. However, the $|\omega_-^+\rangle$ and $|\omega_+^-\rangle$ modes of Ag–ITO–CdS–SiO_2 nanoshells are more sensitive and obvious than those of the Au–ITO–CdS–SiO_2 nanoshells, in which the specific $|\omega_+^-\rangle$ mode is invisible. The mechanism is likely the stronger and sharper surface plasmon resonance of Ag nanoparticles in comparison with that of Au nanoparticles. Based on this mechanism, the metal outer layer of nanoshells influences largely the total plasmon resonance of the multilayered nanoshells and consequently, the $|\omega_+^-\rangle$ mode of the Ag–ITO–CdS–SiO_2 nanoshells becomes intense and noticeable.[8]

3.4. *Effects of shell thickness on extinction spectra*

To obtain more accurate simulation results, DDA-based models that consider the effect of tuning the component thickness on LSPR are developed. The parameters of the Ag-coated ITO–CdS–SiO_2 multilayered nanoshells are $[r_2, r_3 - r_2, r_4 - r_3] = [15, 10, 10]$ nm and $n = 1.0$, with r_1 between 5 nm and 25 nm. Figure 6(a) shows that the $|\omega_-^-\rangle$ mode

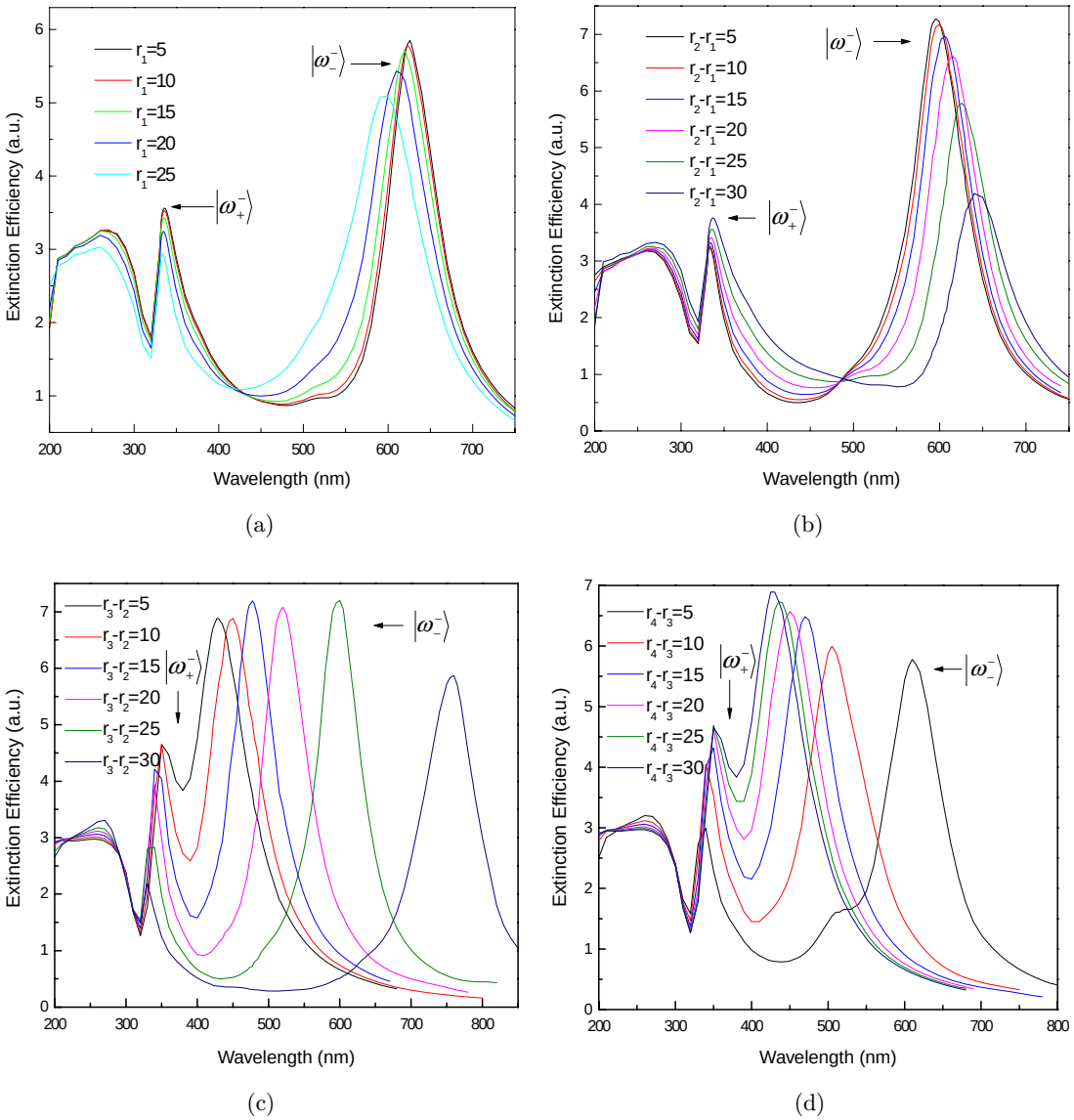

Fig. 6. Calculated extinction spectra of Ag–ITO–CdS–SiO_2 multilayered nanoshells as a function of refractive index of the surrounding medium with different (a) SiO_2 core thickness; (b) CdS inner shell thickness; (c) ITO middle shell thickness; and (d) silver outer shell thickness.

blue-shifts from 626 nm to 595 nm as the SiO_2 core radius increases. The resonance wavelength of the $|\omega_+^-\rangle$ mode shows a small blue-shift relative to the SiO_2 core radius.

The effect of different CdS inner shell thicknesses on extinction spectrum is examined by fixing $[r_1, r_2, r_4 - r_3] = [5, 40, 10]$ nm, as shown in Fig. 6(b). The $|\omega_-^-\rangle$ mode blue-shifts from 640 nm to 595 nm when the thickness of the CdS inner shell increases from 5 nm to 30 nm, while the extinction efficiency diminishes gradually, indicating that the $|\omega_-^-\rangle$ mode is sensitive to the thickness of the CdS inner shell. In the $|\omega_-^-\rangle$ mode, the bonding metal shell plasmon is affected by hybridization of the SiO_2 core, ITO middle shell and CdS shell. By controlling the thickness of the CdS inner shell, the interaction between the SiO_2 core and Ag outer shell can be tailored arbitrarily.[28] When the thickness of the CdS inner shell increases, the interaction of the metal shell plasmons decreases, leading to blue-shifted plasmonic bands. The parameters of the Ag–ITO–CdS–SiO_2 multilayered nanoshells are also defined as $[r_1, r_2 - r_1, r_4] = [5, 10, 50]$ nm. Increasing the ITO middle shell thickness leads to red-shift in the $|\omega_-^-\rangle$ mode from 428 nm to 760 nm, whereas the $|\omega_+^-\rangle$ mode blue-shifts, as shown in Fig. 6(c). The extinction spectra of the Ag–ITO–CdS–SiO_2 multilayered nanoshells with different Ag outer shell thicknesses are plotted in Fig. 6(d). The parameters are $[r_1, r_2 - r_1, r_3 - r_2] = [5, 5, 10]$ nm. The $|\omega_-^-\rangle$ mode blue-shifts from 610 nm to 425 nm when the thickness of Ag shell changes from 5 nm to 30 nm, whereas the $|\omega_+^-\rangle$ mode red-shifts.

4. Conclusion

In summary, the optical properties of Ag–ITO–CdS–SiO_2 nanoshells are simulated by the DDA method and the following conclusions can be drawn:

(1) The electric field enhancement contours of the surface resonance wavelength show the $|\omega_+^-\rangle$ mode at a shorter wavelength corresponding to the symmetric coupling between the anti-bonding silver shell plasmon mode and inner sphere plasmon, while the $|\omega_-^-\rangle$ and $|\omega_-^+\rangle$ modes at longer wavelengths are responsible for the symmetric or anti-symmetric coupling between the bonding of silver shell plasmon mode and spherical plasmon.

(2) The $|\omega_-^-\rangle$, $|\omega_-^+\rangle$ and $|\omega_+^-\rangle$ modes red-shift with the refractive index of the surrounding medium increasing. The thicknesses have a large influence on the LSPR properties of the nanoparticles. Increasing the thickness of the SiO_2 core, CdS inner shell and Ag outer shell blue-shifts the LSPR peak. Although the SiO_2 core reduces the extinction efficiency, the CdS inner shell and Ag outer shell exhibit higher extinction efficiency. On the contrary, the thickness of the ITO middle shell causes red-shift of the peak of LSPR.

(3) By comparing the extinction efficiency spectra of Au–ITO–CdS–SiO_2 and Ag–ITO–CdS–SiO_2 multilayer nanoshells, the $|\omega_-^-\rangle$ mode of the Ag-coated nanoshell blue-shifts. Simultaneously, the $|\omega_+^-\rangle$ and $|\omega_-^+\rangle$ modes of the Ag-coated multilayered nanostructure become intense and noticeable.

Acknowledgments

This work was supported by the National Natural Science Foundation of China (51474069, 51374072), Program for New Century Excellent Ta-lents in Heilongjiang Provincial University (1253-NCET-002), Research project of science and technology of Heilongjiang Province (12541053, 12541096) and City University of Hong Kong Applied Research Grant (ARG) No. 9667104.

References

1. Y. H. Song, J. S. Luo, Y. Yi, K. Li, X. L. Tan, B. C. Luo, X. B. Xu and H. L. Lei, *Chem. Phys. Lett.* **614**, 21 (2014).
2. A. D. Khan, S. D. Khan, R. U. Khan and N. Ahmad, *Plasmonics* **9**, 461 (2014).
3. X. H. Xia, Y. Liu, V. Backman and G. A. Ameer, *Nanotechnology* **17**, 5435 (2006).
4. H. L. Duan and Y. M. Xuan, *Physica E* **43**, 1475 (2011).
5. J. Katyal and R. K. Soni, *Plasmonics* **9**, 1171 (2014).
6. O. Peña-Rodríguez and U. Pal, *Nanoscale Res. Lett.* **6**, 279 (2011).
7. J. Zhu, J. J. Li and J. W. Zhao, *Plasmonics* **8**, 1493 (2013).
8. R. Singh and R. K. Soni, *Appl. Phys. A.* **116**, 955 (2014).
9. V. Myroshnychenko, J. Rodríguez-Fernández, I. Pastoriza-Santos, A. M. Funston, C. Novo, P. Mulvaney, L. M. Liz-Marzán and F. Javier García de Abajo, *Chem. Soc. Rev.* **37**, 1792 (2008).

10. J. F. Ho, B. Luk'yanchuk and J. B. Zhang, *Appl. Phys. A.* **107**, 133 (2012).
11. Y. Zhang, X. G. Yin and M. Han, *J. Opt.* **15**, 1 (2013).
12. K. D. Osberg, N. Harris and T. Ozel, *Nano. Lett.* **14**, 6949 (2014).
13. K. H. Su, Q. H. Wei and X. Zhang, *Appl. Phys. Lett.* **88**, 063118 (2006).
14. J. Qian, Z. Q. Chen, W. D. Wang, Y. D. Li, J. J. Xu and Q. Sun, *Plasmonics* **9**, 1361 (2014).
15. A. Kumar, R. Srivastava, P. Tyagi, M. N. Kamalasanan and D. S. Mehta, *Org. Electron.* **13**, 2879 (2012).
16. T. O. L. Sunde, M. A. Einarsrud and T. Grande, *J. Eur. Ceram. Soc.* **33**, 565 (2013).
17. A. Soleimani-Gorgani, E. Bakhshandeh and F. Najafi. *J. Eur. Ceram. Soc.* **34**, 2959 (2014).
18. H. A. Abbas, A. M. Youssef, F. F. Hammad, A. M. A. Hassan and Z. M. Hanafi, *J. Nanopart. Res.* **16**, 2518 (2014).
19. D. Mandal and U. Chatterjee, *J. Chem. Phys.* **126**, 1 (2007).
20. E. Prodan, C. Radloff, N. J. Halas and P. Nordlander, *Science* **302**, 419 (2003).
21. C. Noguez, *J. Phys. Chem. C* **111**, 3806 (2007).
22. A. L. Gonzalez, C. Noguez and G. P. Ortiz, *J. Phys. Chem. B* **109**, 17512 (2005).
23. H. Duan and Y. Xuan, *Sol. Energ. Mater. Sol. C.* **8**, 121 (2014).
24. D. E. Palik, *Handbook of Optical Constant of Solids*, Part 2 (Academic Press Inc., 1985).
25. A. Chahadih, H. E. Hamzaoui and O. Cristini, *Nanoscale. Res. Lett.* **7**, 487 (2012).
26. L. Baia and S. Simon, *Mod. Res. Educ. Top. Microsc.* **2**, 576 (2007).
27. E. Rodil, L. Aldous and C. Hardacre, *Nanotechnology* **19**, 1 (2008).
28. C. Radloff and N. J. Halas, *Nano. Lett.* **4**, 1323 (2004).
29. Y. Zhang, G. T. Fei and L. D. Zhang, *J. Appl. Phys.* **109**, 054315 (2011).
30. F. Shirzaditabar and M. Saliminasab, *Phys. Plasmas.* **20**, 052109 (2013).
31. X. B. Xu, Z. Yi, X. B. Li, Y. Y. Wang, X. Geng, J. S. Luo, B. C. Luo, Y. G. Yi and Y. J. Tang, *J. Phys. Chem. C* **116**, 24046 (2012).
32. J. Zhu, J. J. Li and J. W. Zhao, *Plasmonics* **6**, 527 (2011).